Matrix Biology Plus 23 (2024) 100157

Contents lists available at ScienceDirect

Matrix Biology Plus

journal homepage: www.sciencedirect.com/journal/matrix-biology-plus

Cartilage-derived cells display heterogeneous pericellular matrix synthesis in agarose microgels

Marloes van Mourik [a,b], Bart M. Tiemeijer [b,c], Maarten van Zon [a], Florencia Abinzano [a,b], Jurjen Tel [b,c], Jasper Foolen [a,b], Keita Ito [a,b,*]

[a] Orthopaedic Biomechanics, Department of Biomedical Engineering, Eindhoven University of Technology, Gem-Z 1.106, P.O. Box 513, 5600 MB Eindhoven, the Netherlands
[b] Institute for Complex Molecular Systems, Eindhoven University of Technology, 5600 MB Eindhoven, the Netherlands
[c] Laboratory of Immunoengineering, Department of Biomedical Engineering, Eindhoven University of Technology, 5600 MB Eindhoven, the Netherlands

ARTICLE INFO

Keywords:
Chondrocytes
Chondroprogenitors
Pericellular matrix
Type-VI collagen
Perlecan
Microgels

ABSTRACT

The pericellular matrix (PCM) surrounding chondrocytes is essential for articular cartilage tissue engineering. As the current isolation methods to obtain chondrocytes with their PCM (chondrons) result in a heterogeneous mixture of chondrocytes and chondrons, regenerating the PCM using a tissue engineering approach could prove beneficial. In this study, we aimed to discern the behavior of articular chondrocytes (ACs) in regenerating the PCM in such an approach and whether this would also be true for articular cartilage-derived progenitor cells (ACPCs), as an alternative cell source. Bovine ACs and ACPCs were encapsulated in agarose microgels using droplet-based microfluidics. ACs were stimulated with TGF-β1 and dexamethasone and ACPCs were sequentially stimulated with BMP-9 followed by TGF-β1 and dexamethasone. After 0, 3, 5, and 10 days of culture, PCM components, type-VI collagen and perlecan, and ECM component, type-II collagen, were assessed using flow cytometry and fluorescence microscopy. Both ACs and ACPCs synthesized the PCM before the ECM. It was seen for the first time that synthesis of type-VI collagen always preceded perlecan. While the PCM synthesized by ACs resembled native chondrons after only 5 days of culture, ACPCs often made less well-structured PCMs. Both cell types showed variations between individual cells and donors. On one hand, this was more prominent in ACPCs, but also a subset of ACPCs showed superior PCM and ECM regeneration, suggesting that isolating these cells may potentially improve cartilage repair strategies.

Introduction

Articular hyaline cartilage regeneration is a long-standing challenge with significant implications for joint homeostasis. If left untreated, local chondral defects significantly increase the risk of developing osteoarthritis [1]. Thus, finding adequate cartilage repair techniques is relevant. Cell-based approaches for cartilage repair, like autologous chondrocyte implantation (ACI), use articular chondrocytes (ACs) harvested from a cartilage biopsy taken from the patient [2]. Despite the relief of clinical symptoms, the use of ACs often results in fibrocartilaginous tissue development with inferior properties and longevity compared to the native tissue [3,4]. The two main causes of failure are the loss of the chondrogenic phenotype during expansion [5] and the loss of the native cell microenvironment [6].

Embedded in their native tissue, ACs are surrounded by a thin layer of highly specialized pericellular matrix (PCM), which are together called the chondron. The chondron is considered to be the functional unit of articular cartilage, as the PCM is essential for the transduction of biophysical stimuli to the cells [7–9]. Type-VI collagen and perlecan are considered essential PCM components, as the colocalization of these proteins has imperative effects on PCM stiffness [10,11]. Additionally, perlecan can modulate the activity of growth factors [12].

During cartilage regeneration, ACs are known to produce PCM before the functional extracellular matrix (ECM) [13], stressing the importance of the presence of an appropriate cell microenvironment. Not surprisingly, chondron-based approaches lead to more effective outcomes

Abbreviations: AC, articular chondrocyte; ACPC, articular cartilage-derived progenitor cells; MFI, mean fluorescence intensity.

* Corresponding author at: Orthopaedic Biomechanics, Department of Biomedical Engineering, Eindhoven University of Technology, Gem-Z 1.106, P.O. Box 513, 5600 MB Eindhoven, the Netherlands.
E-mail addresses: m.v.mourik@tue.nl (M. van Mourik), f.abinzano@tue.nl (F. Abinzano), j.tel@tue.nl (J. Tel), jfoolen@tue.nl (J. Foolen), k.ito@tue.nl (K. Ito).

https://doi.org/10.1016/j.mbplus.2024.100157
Received 17 April 2024; Received in revised form 4 July 2024; Accepted 11 July 2024
Available online 15 July 2024
2590-0285/© 2024 The Author(s). Published by Elsevier B.V. This is an open access article under the CC BY-NC-ND license (http://creativecommons.org/licenses/by-nc-nd/4.0/).

compared to bare ACs [14–16]. However, enzymatic isolation of chondrons results in low yields, heterogeneous cell populations [17,18], and the loss of important matrix components [19]. This increases the demand for alternative methods of obtaining or producing chondrons. An *in vitro* tissue engineering approach could provide a potential solution.

Since *in vitro* expansion of ACs leads to the loss of the chondrogenic phenotype, alternative cell sources have been extensively explored. The use of mesenchymal stromal cells (MSCs) is widespread in literature as they are readily available as an autologous cell source [20,21]. However, using MSCs is often associated with hypertrophic differentiation and the formation of fibrocartilage and calcified cartilage [22]. Another potential cell source is articular cartilage-derived progenitor cells (ACPCs). These cells have major benefits over both ACs and MSCs as they keep their chondrogenic potential even after extensive passaging [23,24] and refrain from hypertrophic differentiation [25]. Additionally, there are reports that ACPCs have superior capabilities to form neocartilage when compared to ACs [26]. Considering that a PCM is required for ACs to produce their ECM, it is hypothesized that the same holds for ACPCs. However, since there are only very limited reports on PCM formation by ACPCs [27], the ability of ACPCs to produce a PCM still has to be investigated in more detail.

To assess PCM synthesis by ACs and ACPCs, hydrogels are the most promising platform. ACs are known to produce and maintain their PCM in agarose hydrogels [28], making agarose a suitable material. The use of micro-scale agarose hydrogels allows for the quantitative analysis of matrix synthesis by single cells or small cell clusters using multiparameter flow cytometry [29]. Using such a platform will allow the exploration of a temporal sequence in the production of different matrix components.

In this study, we aim to regenerate the cartilage PCM using an *in vitro* tissue engineering approach. To assess their potential as an alternative to ACs, the ability of ACPCs to produce a PCM will also be investigated. We hypothesize that, like ACs, ACPCs produce PCM components before ECM synthesis. Due to ACPC's enhanced capacity to produce ECM, we anticipate PCM synthesis to resemble that of ACs, preceding ECM synthesis. Sequential stimulation with bone morphogenic protein-9 (BMP-9) and transforming growth factor-β (TGF-β) was used to enhance the chondrogenic potential of ACPCs [30,31]. Agarose microgels manufactured with droplet-based microfluidics were used as a carrier for ACs and ACPCs, enabling the analysis of differences in matrix synthesis by individual cells and small cell clusters. Since ACPCs are a selected cell population, it is expected that these cells show more homogeneous cell behavior compared to ACs. To evaluate PCM and ECM synthesis, type-VI collagen, perlecan, and type-II collagen produced in the cell-laden microgels was analyzed using flow cytometry and fluorescence microscopy.

Results

Droplet-based single-cell microencapsulation allows for high-resolution analyses

To facilitate a homogeneous microenvironment during *in vitro* culture, ACs and ACPCs were encapsulated in agarose microgels using droplet-based microfluidics. Analysis of the droplets showed that the highest percentage of cell-laden microgels contained one cell (AC: 23.0 % (±7.56; n = 20); ACPC: 25.1 % (±5.37; n = 21)), following the calculated Poisson's distribution (Fig. 1A, B). The mean size of the droplets containing ACs and ACPCs was 66.3 μm (±4.38; n = 200) and 65.8 μm (±3.72; n = 240), respectively (Fig. 1C). A batch of droplets was

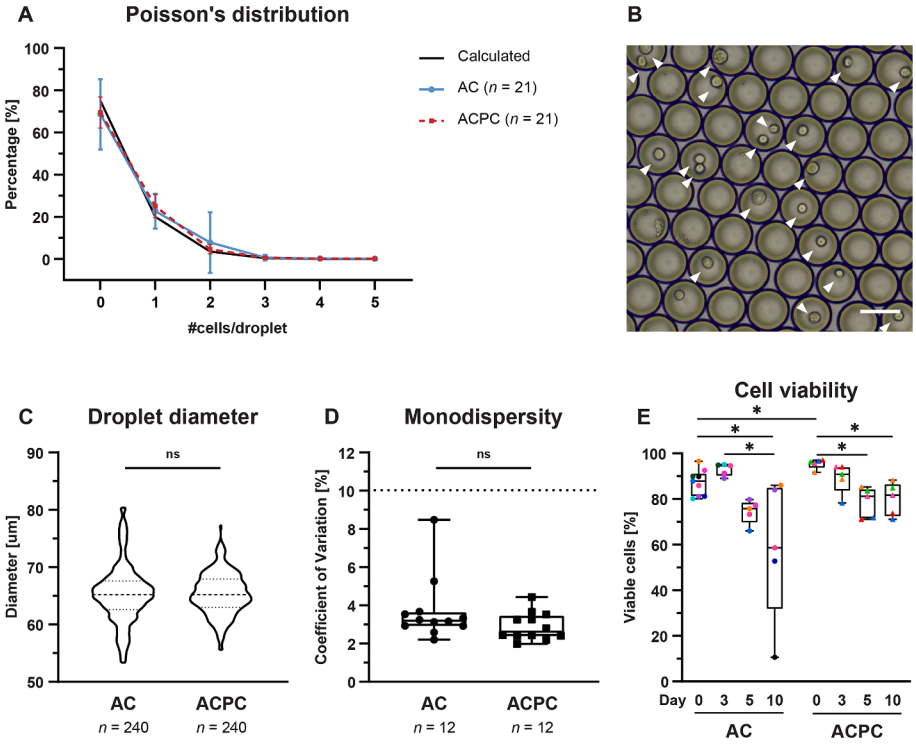

Fig. 1. Cell type does not influence the encapsulation characteristics of agarose microgels. A: Calculated and measured Poisson's distribution for ACs and ACPCs. Line graph with mean and SD at each data point. B: Representative microscopy image of cell-laden agarose droplets in emulsion before gelation. Cells are indicated with arrowheads. Scale bar = 50 μm. C: Violin plot showing the size distribution of the microgels. Unpaired t-tests showed no significant difference between ACs and ACPCs. D: Box and whiskers plot of coefficient of variation in droplet size. Batches were considered monodisperse when CV < 10 %. Unpaired t-tests showed no significant differences between ACs and ACPCs. E: Viability of ACs and ACPCs on days 0, 3, 5, and 10. The % of viable cells is based on DAPI presence and FACS analysis with symbol colors corresponding to donors (uniform across all figures). Time points were compared with a mixed-effects analysis (ACs) or a Friedman test (ACPCs). Cell types were compared with an independent *t*-test (day 3, 5, 10) or a Mann-Whitney test (day 0). Box and whisker plots show the median, first quartiles, and minimum and maximum values. * $p < 0.05$; ns: not significant.

considered monodisperse when the coefficient of variation (CV) of the droplet size was < 10 %. Both cell types resulted in monodisperse batches as the CV of the droplets containing ACs and ACPCs was 3.83 % (±1.74; $n = 11$) and 2.91 % (±0.73; $n = 12$), respectively (Fig. 1D). No significant differences were observed in Poisson distribution, droplet diameter (AC: 65.4 μm ± 5.08; ACPC: 65.4 μm ± 3.64; $p > 0.9999$), and monodispersity (AC: 3.72 % ± 1.68; ACPC: 2.91 % ± 0.73; $p = 0.142$) between microgels containing ACs or ACPCs.

Based on the analysis of DAPI staining using FACS, cell viability could be determined at the moment of analysis. Cells remained largely viable during culture (Fig. 1E). The cell viability of ACPCs on day 0 (95.4 ± 2.15 %) was significantly higher than ACs on day 0 (87.5 ± 5.85 %; $p = 0.028$), but was significantly decreased on day 5 (78.6 ± 6.67 %; $p = 0.0036$) and day 10 (79.9 ± 7.33 %; $p = 0.042$). However, the viability of the ACs at day 10 (58.4 % ± 30.6) significantly decreased compared to day 0 (87.5 % ± 5.85 %; $p = 0.013$) and day 3 (92.98 % ± 2.71 %; $p = 0.012$). This can be attributed to the large donor variability in the cell viability of ACs on day 10. One sample of ACs on day 10 showed an extremely low cell viability of 10.6 %. As the effect of such low cell viability on other readouts is unclear, this particular sample was excluded from further analyses.

Encapsulated ACs and ACPCs rapidly produce PCM and ECM

To assess the synthesis of PCM (type-VI collagen and perlecan) and ECM (type-II collagen) components, fluorescent antibody staining for these matrix proteins were analyzed using flow cytometry and fluorescent microscopy. Additionally, a semi-quantitative analysis was performed on the fluorescent microscopy images to assess the structural quality of the produced PCM. The flow cytometry analysis (Fig. 2) and fluorescence microscopy (Fig. 4) showed rapid production of PCM by both ACs and ACPCs. Due to the large variance between donors, only the MFI values for type-VI collagen for ACs significantly increased between day 3 (7.79 ± 2.81) and day 10 (28.9 ± 16.5; $p = 0.047$). Additionally, the perlecan MFI (Fig. 2B) significantly increased for ACPCs between day 3 (16.0 ± 8.66) and day 10 (44.0 ± 41.85; $p = 0.034$), despite the large variations between donors. Even though no other statistical significances were found, trends of increasing MFI were visible for all proteins.

As not all microgels contained the same number of cells, a semi-quantitative analysis of the microscopy data was used to determine the relative area of type-VI collagen and perlecan staining to the area of DAPI staining. These results showed that the number of cells per microgel possibly influenced the results of the flow cytometry analysis. No significant differences were found for the relative area of type-VI collagen staining (Fig. 3A). The relative area of perlecan staining significantly increased for ACPCs on day 5 (0.39 ± 0.10; $p = 0.029$) and day 10 (1.30 ± 0.19; $p = 0.016$) compared to day 3 (0.39 ± 0.76). Additionally, the relative area of perlecan was significantly higher for ACs on day 3 (1.01 ± 0.34; $p = 0.013$), but not on the other time points. Together with the flow cytometry analysis (Fig. 2B), these results indicate that ACPCs produce less perlecan in the early time points than ACs, but reach similar levels after day 5.

Surprisingly, ACPCs showed large variations between donors in the normalized MFI of the two PCM components (Fig. 2A, B). While most data points fell in a similar range to the ACs, one sample exceeded the others with normalized MFI three times higher for both type-VI collagen and perlecan. This indicated larger variability between ACPC donors when compared to ACs. As seen with the PCM components, there was large donor variability in the production of type-II collagen. This can especially be seen for ACs and ACPCs at day 10 when comparing the normalized MFI's (Fig. 2C). Both cell types showed samples with normalized MFI's in the lower and higher ranges. This indicated that some donors were capable of synthesizing ECM earlier compared to other donors. Additionally, when comparing the two cell types on day 5, the variation of ACPCs was much larger compared to ACs, with the maximum normalized MFI value of ACPCs exceeding the maximum normalized MFI of ACs. This indicated that some ACPC donors were able to synthesize ECM earlier compared to ACs and other ACPC donors. These observations were supported by the microscopy data (Fig. 4).

Flow cytometry and microscopy suggest that matrix synthesis is a sequential process

To have a more in-depth analysis of the co-synthesis of the matrix components, flow cytometry data was plotted with quad gates, based on the day 0 control samples. For visualization, all parameters were normalized to these set gates. This eliminates the donor variability and allows for the comparison of the fluorescence patterns of all samples. The outer contours of each donor were plotted on the dot plots.

The patterns of the flow cytometry data suggested that cells produced matrix components in a sequential manner, which applied to both the ACs and ACPCs. When comparing the two PCM components, type-VI collagen and perlecan, the flow cytometry data showed that type-VI collagen preceded perlecan synthesis (Fig. 5C-J). This can be observed by the change of localization of the events in the quadrants over time. The quadrants in the presented dot plots are based on day 0 staining (the baseline). For both ACs and ACPCs, the dot plots showed that all events are in Q4 (double negative), Q1 (only type-VI collagen positive), or Q2 (double positive). The number of events in Q3 (only perlecan positive) was negligible. Over the culture period, the majority of the cells move from Q4 on day 0, via Q1 on day 3, to Q2 on days 5 and 10. This general

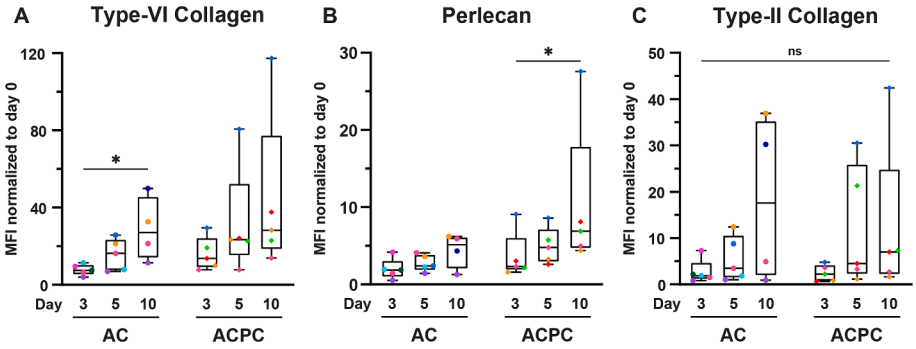

Fig. 2. PCM and ECM components are rapidly synthesized by ACs and ACPCs but with large donor variability. MFI values normalized to day 0 for type-VI collagen (A), perlecan (B), and type-II collagen (C) representing synthesis of these matrix components by ACs and ACPCs after 3, 5, and 10 days of culture in agarose microgels with symbol colors corresponding to donors (uniform across all figures). Time points were compared with a mixed-effects analysis (ACs: type-VI collagen, perlecan), a Kruskal-Wallis test (ACs: type-II collagen) or a Friedman test (ACPCs: all markers). Cell types were compared with an independent *t*-test (type-VI collagen: day 3; perlecan: day 5; type-II collagen: day 5) or a Mann-Whitney test (type-VI collagen: day 5, 10; perlecan: day 3, 10; type-II collagen: day 3, 10). Box and whisker plots show the median, first quartiles, and minimum and maximum values. * $p < 0.05$; ns: not significant.

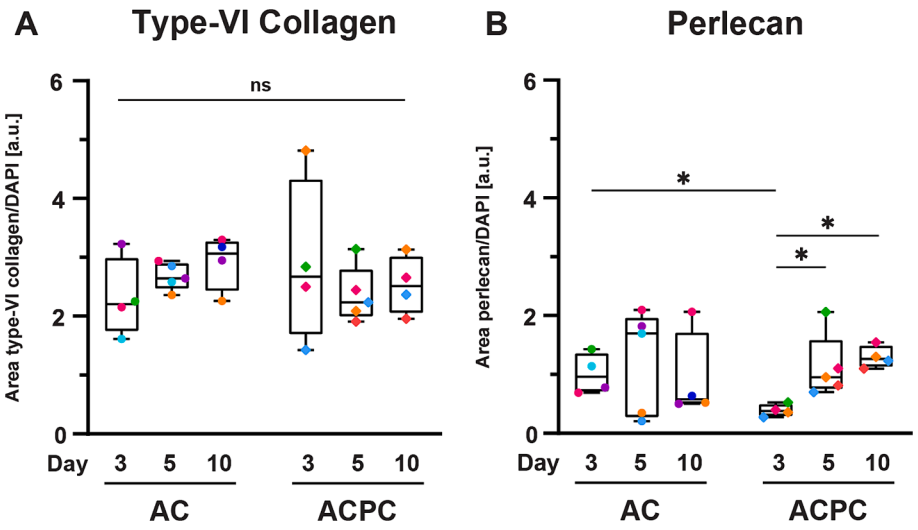

Fig. 3. The stained area of type-VI collagen (A) and perlecan (B) relative to the area of DAPI staining indicates that the amount of matrix produced does not increase with the cell content (with symbol colors corresponding to donors, uniform across all figures). Time points were compared with a mixed-effects analysis (ACs: type-VI collagen; ACPCs: all markers) or a Kruskal-Wallis test (ACs: perlecan). Cell types were compared with an independent *t*-test (type-VI collagen: all time points; perlecan: day 3, 5) or a Mann-Whitney test (perlecan: day 10). Box and whisker plots show the median, first quartiles, and minimum and maximum values. * $p < 0.05$; ns: not significant.

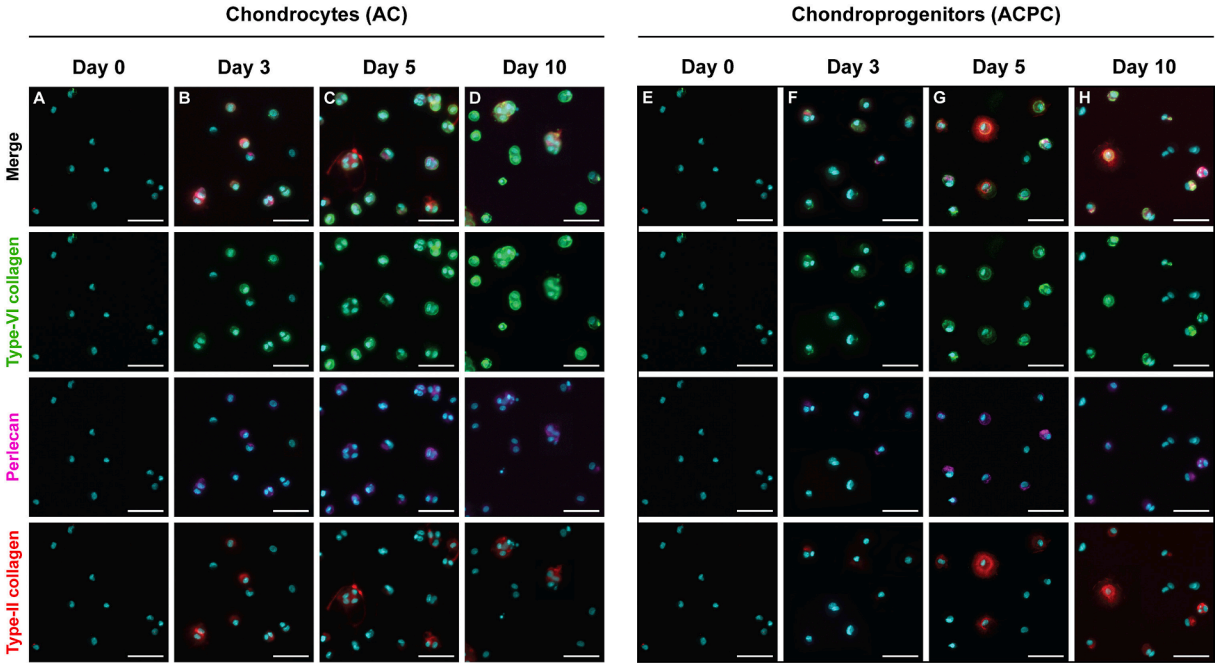

Fig. 4. Both ACs and ACPCs produce PCM and ECM components, but there are differences in structure and production rates by individual cells. Representative fluorescence microscopy images of ACs (A-D) and ACPCs (E-H) in agarose microgels showing the presence of PCM and ECM components at days 0, 3, 5, and 10. Tiles show DAPI (cyan) with either type-VI collagen (green), perlecan (violet), type-II collagen (red), or a merged view of all four channels. Scale bar = 50 μm. (For interpretation of the references to color in this figure legend, the reader is referred to the web version of this article.)

trajectory has been projected in Fig. 5A.

In agreement with the flow cytometry results, the microscopy results illustrated similar phenomena. Fig. 5A and B exemplify the relation between the quadrants and the microscopy data, showing cells that can likely be allocated to the labelled quadrants. Microscopy images matching dot plots for both cell types and at all time points have been provided as a Supplementary figure (Fig. S1). When comparing the type-VI collagen and perlecan stainings, perlecan always co-located with cells that also produced type-VI collagen, but not the other way around.

When using the same analysis to compare type-II collagen to either type-VI collagen or perlecan, the results suggest that both PCM components were synthesized before type-II collagen was produced (Figs. S2 and S3). Type-II collagen was only observed when cells were positive for both type-VI collagen and perlecan. These results are confirmed by microscopy data (Fig. 4).

Cell populations of ACPCs display a more heterogeneous synthesis of matrix components than ACs

Although the general patterns of expression seem similar between

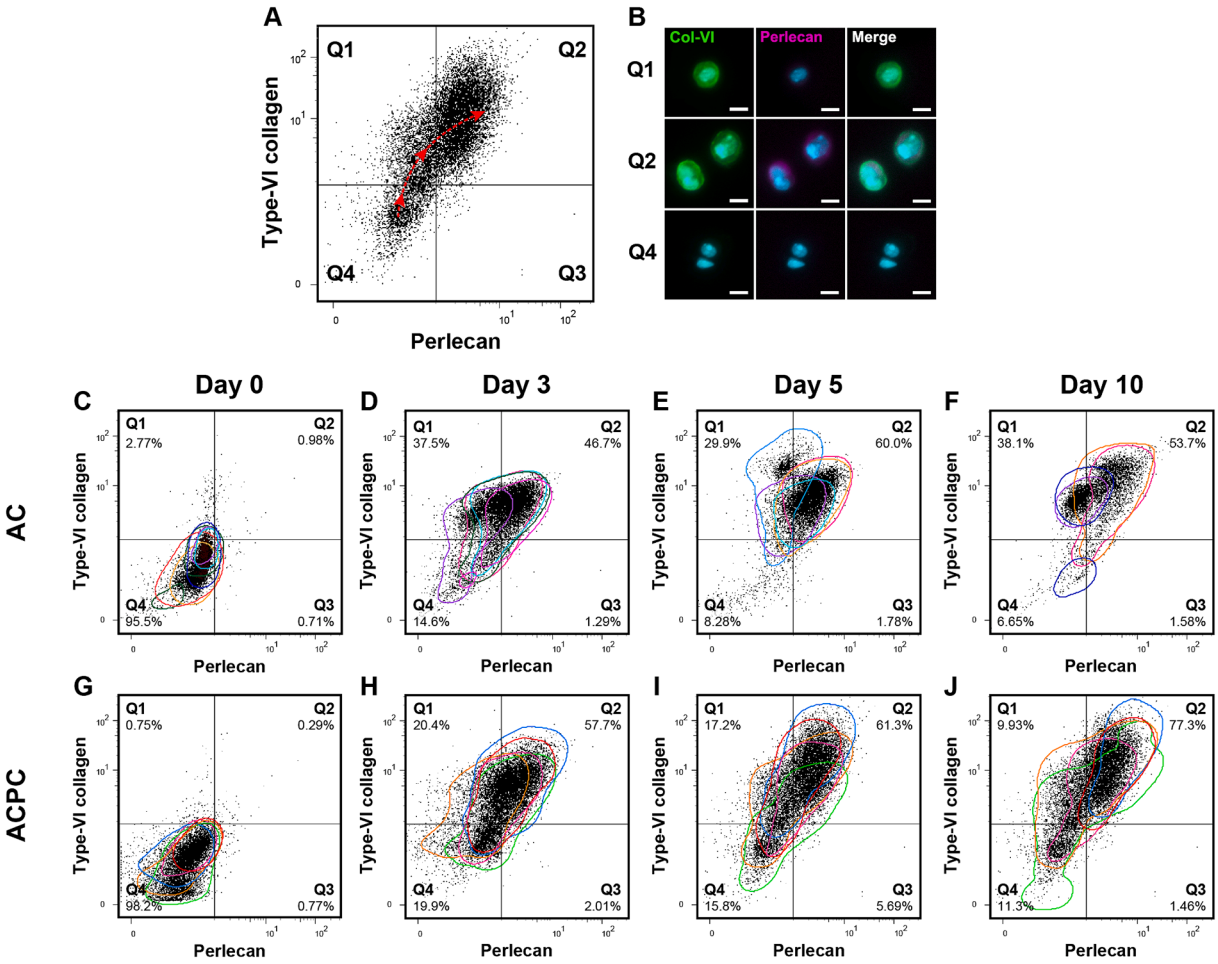

Fig. 5. Flow cytometry dot plots show the relation between type-VI collagen and perlecan, suggesting a sequence in PCM synthesis and highlighting between-donor and within-donor variabilities. The colored contours in the dot plots represent individual donors with colors corresponding to donors (uniform across all figures). A: The quadrants in the dot plots are based on day 0 staining. The quadrants represent microgels without staining (Q4), only type-VI collagen (Q1) or perlecan (Q3), or, both type-VI collagen and perlecan (Q2). The general trajectory of matrix synthesis observed over the culture time has been projected as the dashed line with arrowheads. The microscopy images in B show cells that would likely allocate to Q1, 2, and 4, representing the distribution of the matrix components per quadrant. Scale bar = 10 μm. During culture, ACs (C-F) and ACPCs (G-J) have similar patterns of PCM synthesis, where the presence of type-VI collagen precedes that of perlecan. The colored contours highlight donor variability. The distribution of events over different quadrants shows the variability between individual cells, highlighting heterogeneous cell behavior. Percentages are the mean of each quadrant.

donors and cell types, and the used platform facilitates a homogeneous microenvironment for the cells, a heterogeneous cell response was observed both within the cell populations and between donors. Variations between donors were highlighted by the shift in the differently colored dot plots, which represent the individual donors (Fig. 5). This reflects the distribution of data points of normalized MFIs (Fig. 2).

However, when looking at the flow cytometry data, details in heterogeneity within a cell population could be observed, which were lost when only looking at the normalized MFIs. This variation was most striking when comparing ACPC donors at day 10, where there was a large discrepancy between cells that seemingly did not make any matrix and cells that had produced all three investigated matrix components (Figs. 5, S1-3). Especially the heterogeneous synthesis of the PCM components of ACPCs (Fig. 5G-J) was noteworthy, as this degree of heterogeneity was not observed in the AC populations (Fig. 5C-F), where seemingly most cells synthesized at least some PCM components. As for type-II collagen, both ACs and ACPCs displayed heterogeneity within the same cell pool, visible in microscopy (Fig. 4) and flow cytometry data (S2 and 3).

ACs produce structurally superior PCMs compared to ACPCs

The structure of the formed PCM was analyzed with a semi-quantitative analysis of the microscopy data, generating results describing the percentage of a cell nucleus covered by PCM and the PCM thickness with respect to the nucleus (Fig. 6A). These analyses were performed only on cells that produced a PCM, without considering cells that did not produce a PCM.

When visually comparing the synthesized PCMs of the two cell types, the PCMs of the ACs appeared structurally superior. The type-VI collagen had formed compact, intact rings surrounding the cells (Fig. 3A-D). This observation is supported by the analysis of the PCM coverage (Fig. 6C). ACPCs that did produce a PCM were covered by significantly less PCM compared to ACs on day 5 (AC: 91.2 % ± 4.4 %; ACPC: 72.3 % ± 8.3 %; $p = 0.002$) and day 10 (AC: 88.7 % ± 7.5 %; ACPC: 70.8 % ± 8.1 %; $p = 0.017$). Additionally, the mean distribution of the PCM coverage shows that ACs have relatively more cells with 75–100 % coverage than ACPCs (Fig. 6D). The percentage of ACPC within this region decreased during culture, while the fraction of cells with 0–25 % coverage increased. This indicates that the cells that start producing a PCM after day 3 have an inferior structure compared to the fraction of cells that produced a PCM earlier.

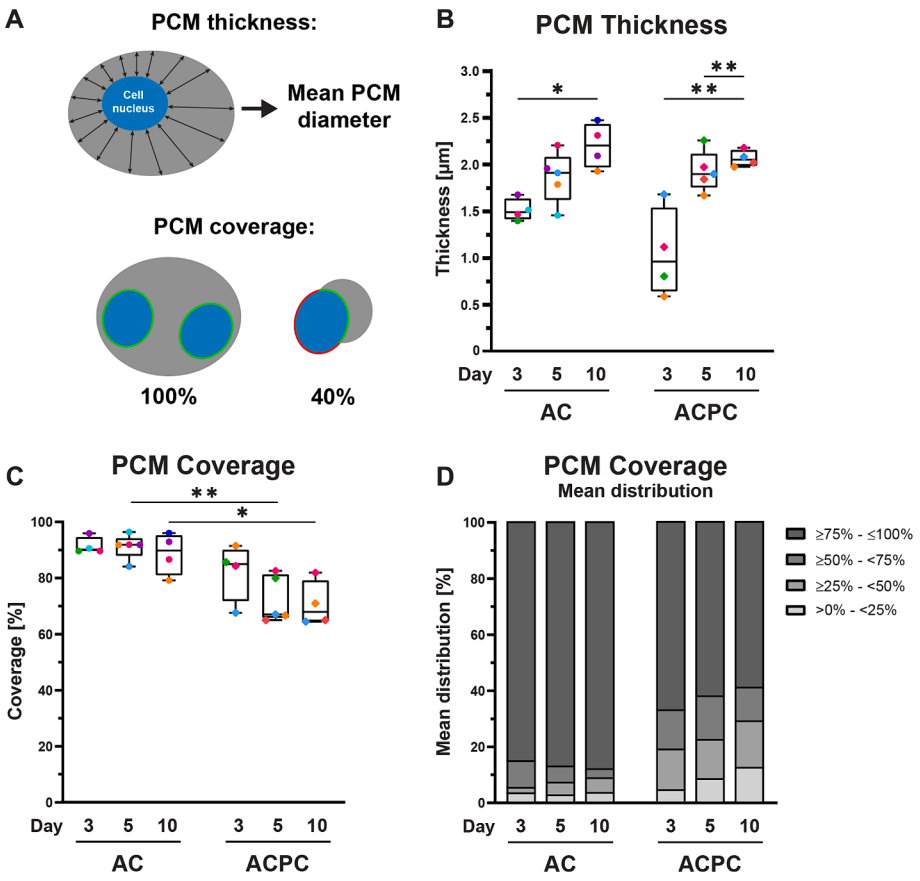

Fig. 6. ACs produce structurally superior PCMs compared to ACPCs based on PCM thickness (B) and coverage (C, D). The PCM thickness was defined as the mean diameter of the PCM, measured from the cell nucleus (A). The PCM coverage is the percentage of the cell nucleus surrounded by type-VI collagen staining, with 100 % defined as full coverage (A). Both parameters exclude cells without a PCM. Symbol colors correspond to individual donors (uniform across all figures). Time points were compared with a mixed-effects analysis (PCM coverage: ACPCs; PCM thickness: ACs, ACPCs) or a Kruskal-Wallis test (PCM coverage: ACs). Cell types were compared with an independent *t*-test (PCM coverage: day 5, 10; PCM thickness: all time points) or a Mann-Whitney test (PCM coverage: day 3). Box and whisker plots show the median, first quartiles, and minimum and maximum values. * $p < 0.05$; ** $p < 0.01$; ns: not significant.

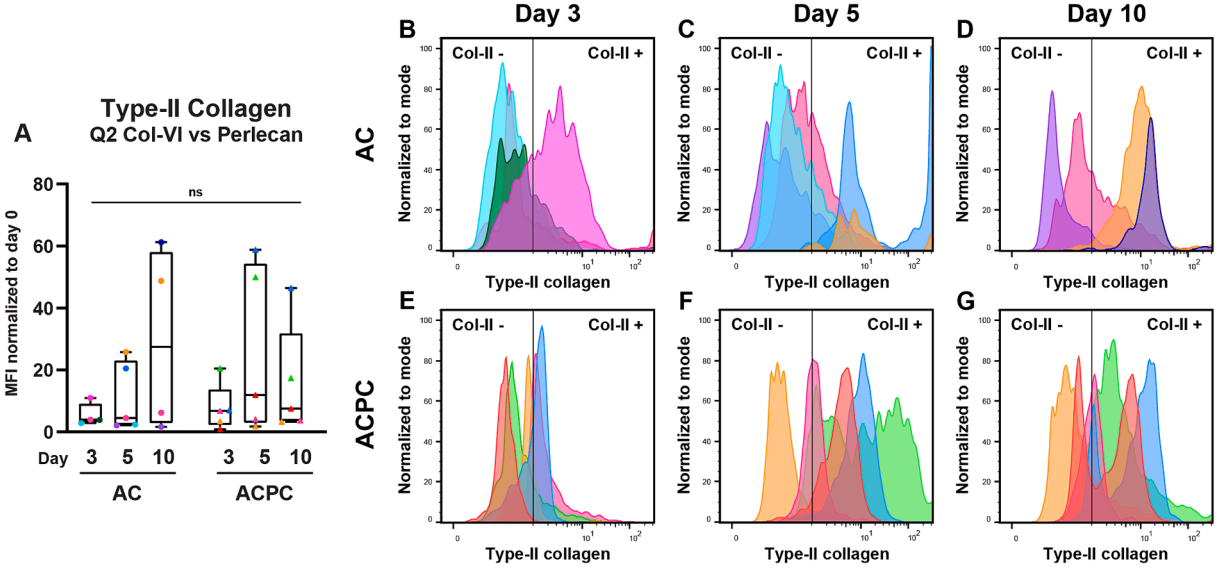

Fig. 7. When producing a complete PCM containing both type-VI collagen and perlecan, a subset of ACPCs can produce type-II collagen earlier than ACs. A: Normalized MFI values of type-II collagen staining for cells that have produced both type-VI collagen and perlecan. This corresponds with the second quadrant as seen in Fig. 5D-F and H-J. Time points were compared with a Kruskal-Wallis test (ACs) or a repeated measures one-way ANOVA (ACPCs). Cell types were compared with a Mann-Whitney test (day 3) or an independent *t*-test (day 5, 10). Box and whisker plots show the median, first quartiles, and minimum and maximum values. ns: not significant. B-G: Histograms of modal type-II collagen intensity in Q2 showing variations between donors and individual cells. The colors represent individual donors (uniform across all figures).

The PCM thickness (Fig. 6B) increased for both cell types, with significant increases for ACs between day 3 (1.52 μm ± 0.12) and day 10 (2.20 μm ± 0.24; $p = 0.0088$) and for ACPCs on day 5 (1.93 μm ± 0.22; $p = 0.0034$) and day 10 (2.07 μm ± 0.09; $p = 0.0018$) compared to day 3 (1.05 μm ± 0.47). No significant differences were found between ACs and ACPCs. These results suggest that both cell types are developing their PCMs during the culture period.

When looking for the "ideal" population for cartilage repair, a subset of ACPCs seems most promising

Synthesis of both PCM and ECM components by the cells is necessary to achieve high-quality neocartilage formation. For this consideration, the synthesis of PCM is the first requirement. From the flow cytometry data, the cells that produce a functional PCM, both type-VI collagen and perlecan, can be identified in the second quadrant (Q2; Fig. 5). However, as can be observed in both the flow cytometry and microscopy data, not all cells that synthesize a PCM also produced type-II collagen at the investigated time points. Therefore, only the cells that had produced a complete PCM containing both type-VI collagen and perlecan were selected to compare the MFI of type-II collagen specifically (Fig. 7A). As not all samples synthesized PCM at the same rate, samples with less than 100 events or less than 10 % of the events in the live gate were considered for this analysis. This resulted in the exclusion of one sample for ACs on day 3. As can be seen, the median MFI values were higher than those of the complete cell populations (Fig. 2C). As was seen for the complete populations, there were again large differences between donors and individual cells. This becomes apparent when comparing the distribution of type-II collagen staining in Q2 (Fig. 7B-G). Interestingly, the distribution of peaks considered type-II collagen positive and negative suggests that when ACPCs produce both type-VI collagen and perlecan, the majority of the cells also produce type-II collagen. This was not observed for the ACs. This was especially apparent on day 5. There was however a large range in the staining intensity, indicating that not all cells produce a similar amount of type-II collagen. This could also be observed in the microscopy results (Fig. 4C, G).

Discussion

The presence of a PCM can alter the transduction of biophysical stimuli to ACs [7–9] and neocartilage formation [13]. As the isolation of chondrons results in a heterogeneous population [17,18], obtaining a more in-depth understanding of PCM formation is essential. Since ACPCs are considered a potential alternative plentiful cell source for cartilage tissue engineering, investigating PCM formation by these cells is also interesting. It was hypothesized that both ACs and ACPCs produce the PCM components type-VI collagen and perlecan before type-II collagen. Additionally, ACPCs were expected to produce a PCM, similar to ACs and show more homogeneous cell behavior. This study shows that, besides the production of the PCM preceding the ECM, there is a distinct sequence in the production of PCM components, with type-VI collagen preceding perlecan. This sequence in matrix synthesis was true for both ACs and ACPCs. Contrary to expectations, ACPCs were found to produce a structurally inferior PCM and displayed more heterogeneity between individual cells when compared to ACs.

Analysis of both the ACs and ACPCs showed the same pattern of matrix synthesis for both cell types. Fluorescent microscopy images (Fig. 4, Fig. 6) and the flow cytometry results (Fig. 5) showed a clear sequence in the synthesis of the analyzed matrix proteins, where the synthesis of type-VI collagen precedes or is simultaneous with that of perlecan. To the authors' knowledge, there is no such clear record of this sequence in the early phases of PCM synthesis in literature yet. Additionally, the PCM components were found to be synthesized before the production of ECM component type-II collagen (Figs. S2, S3). This result agrees with the current literature [13,28,32,33], again emphasizing the relevance of the cell microenvironment for neocartilage formation.

Although type-VI collagen and perlecan are crucial for chondrocyte function, their underlying synthesis mechanisms in chondrocytes have not been thoroughly studied. In fibroblasts, the expression of the COL6A1 and COL6A3 genes is highly dependent on Smad-2/3 signaling, a TGF-β regulated pathway that also has large regulatory effects on type-II collagen and aggrecan [34]. This study however suggests additional regulatory mechanisms, as type-VI collagen synthesis precedes type-II collagen. Nevertheless, from a matrix production point of view, this sequence would be most efficient for retaining the produced perlecan in a peri-cellular nest of collagen type-VI, and understanding these mechanisms could provide a deeper understanding of PCM and ECM synthesis during chondrogenesis and may uncover potential methods to control these processes.

Even though the results showed similar patterns in matrix synthesis by both ACs and ACPCs, some essential differences could be observed. PCMs produced by ACs were compact and thin, resembling native chondrons [35] on day 10 (Fig. 3A-D), which is comparable to PCM formation by human primary chondrocytes in alginate microgels [36,37]. While ACPCs also produced type-VI collagen and perlecan, their PCMs were less organized compared to ACs but did significantly improve over time (Fig. 4E-H, Fig. 6). The coverage of the PCM around ACPCs was significantly lower compared to ACs and the PCMs were less thick on day 3. Additionally, the relative area of perlecan produced by ACPCs was significantly lower on day 3. Since the combined presence of perlecan with type-VI collagen is essential for the mechanical function of the PCM [10,11], these PCMs could be considered immature. However, the amount of perlecan and the PCM thickness did significantly increase on day 10 to similar levels as ACs. The delayed PCM synthesis by ACPCs until day 3 was possibly caused by the lack of TGF-β stimulation until this time point. As BMP-9 stimulation was needed to differentiate the ACPCs, future studies could consider starting a comparison between ACs and ACPCs when both cell types are stimulated with the same growth factors.

Currently, there is little literature on PCM synthesis by ACPCs. One study by Anderson *et al* compared type-VI collagen and perlecan synthesis by human ACs and ACPCs [27]. In contrast to their findings, the PCMs formed by ACs and ACPCs in our study resembled native chondrons more closely. It is worth noting that Anderson *et al* exposed the cells to different conditions, lacking exogenous growth factors and cells were allowed to self-assemble into scaffold-free tissues. As ACs can form well-structured PCMs in alginate without growth factor stimulation [36], the high cell densities in their study might have affected this process. The proximity of the cells could have interfered with PCM formation of neighboring cells as ACs interact with type-VI collagen through integrins. This might have resulted in a lack of pericellular localization, indicating that lower cell densities could be beneficial for PCM formation by ACs.

While ACPCs made better-structured PCMs in their study, they differed significantly from those observed in our study, likely due to the absence of BMP-9 and TGF-β stimulation. Other literature on the effects of these growth factors on PCM synthesis by ACPCs is limited but provides some extra insights. In our study, ACPCs were stimulated for 3 days with BMP-9, which was found to be the most potent factor for chondrogenesis by ACPCs [30]. BMP-9 stimulation upregulates the activity of Smad-1/5/8, but not Smad-2/3 [38,39]. The synthesis of type-VI collagen by ACPCs at day 3 again suggests Smad-independent stimulation of type-VI collagen. Elucidating this mechanism could improve ACPC stimulation and their PCM production.

Aside from the differences in matrix production by ACs and ACPCs, it is evident that both cell types show heterogeneous cell behavior in a homogeneous microenvironment. This heterogeneity was observed both when comparing donors and individual cells within a donor population. This is especially true for PCM synthesis by ACPCs, as can be seen when comparing type-VI collagen and perlecan with flow cytometry (Fig. 5). Interestingly, similar variations between donors and individual cells were observed for both cell types (Figs. 4, S2, S3). ACs are known to

display these variabilities as matrix synthesis is known to be highly dependent on the donor [40] and a cell's zonal origin [41].

Nevertheless, the rationale behind the variations in ACPCs is less straightforward, since the true composition of ACPC populations is still highly debated. Although ACPCs are known to share stem cell markers with MSCs [42], no defined set of markers has been identified to differentiate between ACPCs, MSCs, and even ACs. Therefore the question remains whether ACPCs can be identified as one cell type or a mixture of different cells, making the characterization of these cells crucial [43]. This study showed heterogeneous matrix production by ACPCs, especially type-II collagen. This indicates that ACPCs might not be one cell type but a collection of different cells. As ACPCs can retain their chondrogenic potential even after many passages [23,24], identifying a subset of very potent cells, which could be further expanded, could hold great value for using autologous ACPCs for cell-based cartilage repair. When considering the clinical translation of ACPCs, a main difference in this study should be noted. Exogenous BMP-9 and TGF-β were supplemented during culture, which could be considered less representative of the *in situ* situation. Expanding this research to the use of latent growth factors in the microgel material or other nanocarrier methods could be an interesting course for clinical translation. More in-depth research into the stimulation and population subsets of ACPCs and their implications for clinical translation could result in high-potential cartilage repair applications.

Regardless of the novel insights this study has provided, there are some limitations to the used methods. The viability of both ACs and ACPCs significantly decreased during culture (Fig. 1E), which could indicate that the system is not compatible with these cells. It is hypothesized that the swelling pressure inside the microgels is increased by the production of GAGs, causing them to burst. This could create larger aggregates of cells and matrix, which would be lost during filtering before flow cytometry analysis. This would mean that the cells producing the most matrix are not included in the results on day 10.

The addition of the semi-quantitative analysis of the microscopy data provided more understanding of the structure of newly synthesized PCM. This analysis was based on the segmentation of the obtained microscopy images. However, the quality of the perlecan staining was insufficient to perform a structural analysis based also on this PCM component, since the staining was optimized for flow cytometry. Thus, the structural analysis was restricted to that with collagen-VI. Additionally, since the microscopy data was obtained from the same samples used for flow cytometry first, this data was not collected for all samples. This decreased the sample size of the microscopy analysis.

The amount of PCM and ECM components analyzed was quite limited. When expanding the analysis, adding fibronectin and proteoglycans like aggrecan, chondroitin sulfate, and hyaluronan are valuable since these are major PCM components besides type-VI collagen and perlecan [7,35]. Additionally, analyzing integrins, focal adhesions, and the actin cytoskeleton can elucidate the role of cell-matrix interactions on PCM formation.

Although it would have made for more powerful statistical analysis, it was not possible to harvest all ACs and ACPCs from the same donors. Only 3 donors contributed both cell types, and the other cells came from different donors. The data from each donor are color coded uniformly in all figures, and one can look for consistent correlations of cell performance between donors. Unfortunately, no obvious relationship was evident. Furthermore, primary cells from donors were chosen to reflect more the common clinical approach to cartilage tissue engineering. However, this resulted in larger variability. With a lower biological replicate number, not all observed mean differences were statistically significant. Nevertheless, the conclusions drawn are based on statistically significant quantifiable differences, and the observed differences between ACPCs and ACs should be used with caution until further confirmed.

This study has shown that ACPCs can quickly synthesize the two major PCM components type-VI collagen and perlecan, similar to ACs, although there are differences in their structure. This is the first study to thoroughly analyze the matrix synthesis of cartilage cells using flow cytometry, which showed a distinct synthesis sequence with first type-VI collagen, then perlecan, and finally type-II collagen. Additionally, the current method-derived definition of ACPCs resulted in large variations between individual cell behavior, as well as between donors, despite the homogeneous microenvironment created by the presented culture system. The outcomes of this study will contribute to a deeper understanding of PCM synthesis by ACs and the optimization of ACPC stimulation for their use in cartilage repair.

Experimental procedures

Cartilage digestion and cell isolation

Articular cartilage was isolated and digested from bovine metacarpophalangeal joints (n = 11, AC: n = 9, ACPC: n = 5, age 8–12 months) following a previously described protocol [17]. In summary, articular cartilage was enzymatically digested overnight with 0.15 % collagenase type II (17101-015, Gibco™, Thermo Fisher Scientific, Landsmeer, the Netherlands) and 0.1 % hyaluronidase (H3506, Sigma-Aldrich, Zwijndrecht, the Netherlands) to obtain cartilage-derived cells.

The obtained cells were either subjected to differential fibronectin adhesion to isolate the ACPCs or directly frozen to use as ACs. ACs were frozen in 90 % fetal bovine serum (FBS, BCBV7611, Sigma-Aldrich) and 10 % dimethyl sulfoxide (DMSO, 276855, Sigma-Aldrich) and stored at −150 °C until further use. Before use, ACs were seeded at a density of 2000 cells/cm^2 and expanded until passage 1 for further use.

Chondroprogenitor isolation

The methods of ACPC isolation were modified based on a previously described protocol [30] In short, ACPCs were isolated after the enzymatic digestion of articular cartilage using differential adhesion to fibronectin for 20 min. Nonadherent cells were subsequently removed and the adherent cells were cultured with Dulbecco's Modified Eagle Medium (DMEM) with GlutaMAX™ (31966, Gibco™), 10 % FBS, 1 % penicillin/streptomycin (P/S, m15070063, Thermo Fisher Scientific), 50 μg/mL ascorbic acid-2-phosphate (AsAP, A8960, Sigma-Aldrich), 1 % MEM non-essential amino acids (NEAA, 11140050, Gibco™), and 5 ng/mL recombinant human basic fibroblast growth factor (bFGF, 100-18B, PeproTech, London, United Kingdom). After 5–7 days of culture, at ca. 80 % confluence, cells were released from the culture flask using 0.25 % trypsin-ethylenediaminetetraacetric (EDTA) phenol red solution (25200, Thermo Fisher Scientific). ACPCs were frozen in 90 % FBS and 10 % DMSO and stored at −150 °C until further use. Before use, ACPCs were seeded at a density of 2000 cells/cm2 and expanded until passage 3 for further use.

Fabrication of microfluidic devices

3-Inlet polydimethylsiloxane (PDMS, SYLGARD™ 184, Dow Silicones, Seneffe, Belgium) microfluidic devices were fabricated according to a previously described design (Fig. 8A) and protocol [44]. In short, silicon wafers with 30 μm channel height were produced using soft lithography. PDMS devices were bound to glass slides and channels were made hydrophobic using 5 % 1H,1H,2H,2H-perfluorooctyltriethoxysilane (667420, Sigma-Aldrich) in HFE-7500 fluorinated oil (Novec™ 7500, 3M, Delft, the Netherlands).

Cell microencapsulation and culture

The method to produce cell-laden microgels was based on a previously described protocol [29]. After release from the culture flask, cells were resuspended in 2 mM EDTA in PBS without calcium and magnesium (DPBS, 14190250, Thermo Fisher Scientific) at a concentration of

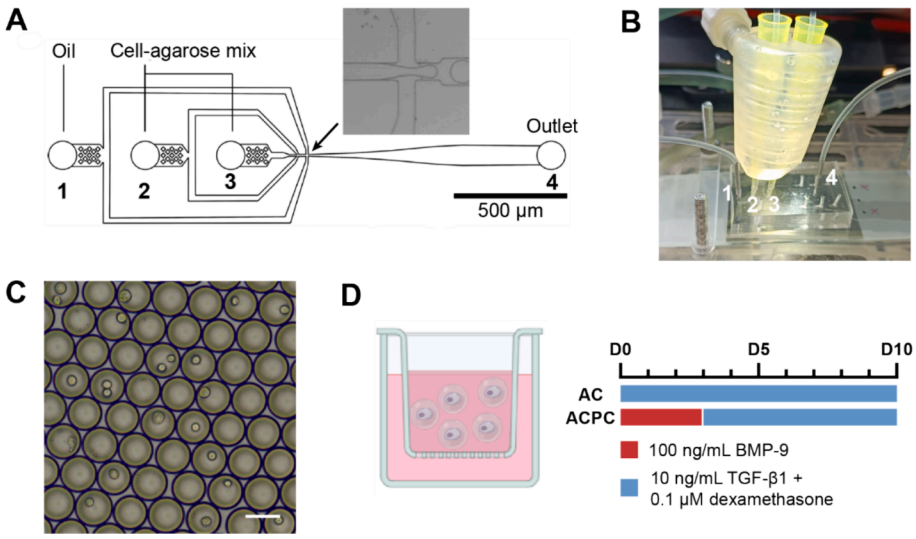

Fig. 8. Overview of the microfluidics setup, cell encapsulation, and culture conditions. A: Microfluidic chip design for droplet-based microgel formation. The arrow indicates the intersection where the emulsion is formed. B: Microfluidics setup showing the PDMS chip, pipette tips containing the cell-agarose mixture, and the heating device. The numbers indicate the inlets and outlet, corresponding with Fig. A. C: Agarose droplets containing cells in emulsion before gelation. Scale bar = 50 µm. D: Schematic image of cell-laden microgels in a culture insert and growth factors added during culture.

10^7 cells/mL. The cell suspension was mixed 1:1 with 2 % w/v ultra-low gelling temperature agarose (A5030, Sigma-Aldrich) in DPBS, resulting in a 1 % w/v agarose solution with $5*10^6$ cells/mL.

The first inlet of the PDMS microfluidic chip was used for the continuous phase, containing 2.5 % (w/v) Pico-Surf surfactant (Sphere Fluidics, Cambridge, United Kingdom) in HFE-7500. The cell-gel solution was loaded into the second and third inlet using the previously described tip-loading technique [44] (Fig. 8A, B). Flow rates of the cell-agarose mix and continuous phase were set to 5 µL/min and 30 µL/min, respectively. The pipette tips and PDMS chip were kept at 37 °C with a custom-made heating device to prevent premature gelation of the agarose (Fig. 8B).

During droplet production, a sample of droplet suspension was collected for imaging with an EVOS™ microscope (Thermo Fisher Scientific) (Fig. 8C). Droplet diameter and cell distribution were determined using ImageJ software. The number of cells was counted per droplet to calculate the distribution of cells, which was compared to the theoretical Poisson distribution [45]. To determine the droplet diameter, 20 droplets were measured per sample. Monodispersity was determined by calculating the coefficient of variation. A batch of droplets was considered monodisperse when the coefficient of variation <10 % [46].

After production, droplet suspension was collected in an Eppendorf tube and the agarose was allowed to gel for 15 min at 4 °C. After gelation, the cell-laden microgels were collected by breaking the oil emulsion using 20 % 1H,1H,2H,2H-perfluoro-1-octanol (PFO, 370533, Sigma-Aldrich) in HFE-7500.

Encapsulated ACs and ACPCs were cultured in 6-well plates loaded with 0.4 µm pore size cell culture inserts (Sterlitech, Auburn, Washington, United States) for 3, 5, or 10 days (Fig. 8D). Culture media contained DMEM (31966), 1 % ITS+premix (354352, Corning™, Life Technologies Europe, Bleiswijk, the Netherlands), 1 % HEPES (15630-080, Gibco™), and 1 % AsAp. ACs were stimulated with 10 ng/mL TGF-β1 (100-21, PeproTech) and 0.1 µM dexamethasone (50-02-2, Merck Life Science NV, Amsterdam, the Netherlands) for 10 days. ACPCs were stimulated with 100 ng/mL BMP-9 (120-07, PeproTech) for 3 days, followed by 10 ng/mL TGF-β1 and 0.1 µM dexamethasone for the remaining 7 days. Culture media was changed every 2–3 days.

Antibody staining and flow cytometry

After culture, cell-laden microgels were collected from the culture inserts and stained with a cocktail of antibodies for type-VI collagen (1:200, FITC-conjugated, 600-402-108, Life Technologies Europe), perlecan (1:200, Alexa Fluor™ 594-conjugated, sc-33707, Santa Cruz Biotechnology, Dallas, Texas, United States), and type-II collagen (1:200, MA512789, Thermo Fisher Scientific). A secondary antibody (1:200, Alexa Fluor™ 647, A21236, Thermo Fisher Scientific) was used for the staining of type-II collagen. All antibodies were incubated for 30 min on ice. Dead cells were stained with 4′,6-diamidino-2-phenylindole (DAPI, 1:5000, D9542, Sigma-Aldrich), as it does not penetrate live cells. Samples were analyzed using FACSymphony A3 (BD Biosciences, Franklin Lakes, New Jersey, United States) and data was analyzed with FlowJo (v 10.9.0, BD Biosciences). Details of the flow cytometry setup are presented in Table S1.

To identify the gate for cell-laden microgels, a batch with empty microgels was compared to a batch with cell-laden microgels (Fig. 9A). Dead cells were excluded, based on a positive DAPI staining (Fig. 9B). Viable cells were used for further analysis. An overview of the number of live events is presented in Table S2. The presence of matrix components was quantified using the geometric mean fluorescence intensity (MFI). The MFI at days 3, 5, and 10 was normalized to day 0 samples to eliminate donor-specific variations in autofluorescence.

Co-presence of the three matrix components was analyzed by plotting two markers and creating quad gates based on the day 0 measurements (Fig. 9C). These gates were copied to the data of days 3, 5, and 10 (Fig. 9D-F). For visualization, all parameters were normalized to these set gates, thus eliminating sample-to-sample differences in fluorescence.

Immunofluorescence microscopy

After analysis with flow cytometry, the samples were fixed with 3.7 % paraformaldehyde in PBS for 15 min and permeabilized with 0.2 % Triton X-100 in PBS for 10 min. Cell nuclei were stained with DAPI (1:500). The suspension was centrifuged and 4 µL samples were taken from the pellet. Samples were placed on a microscopy slide, covered with a cover glass, and visualized using a combination of differential interference contrast microscopy and widefield fluorescent microscopy (20×, 0.4 NA, Axio Observer 7, Zeiss, Oberkochen, Germany).

To determine the relative amount of staining per cell nucleus and

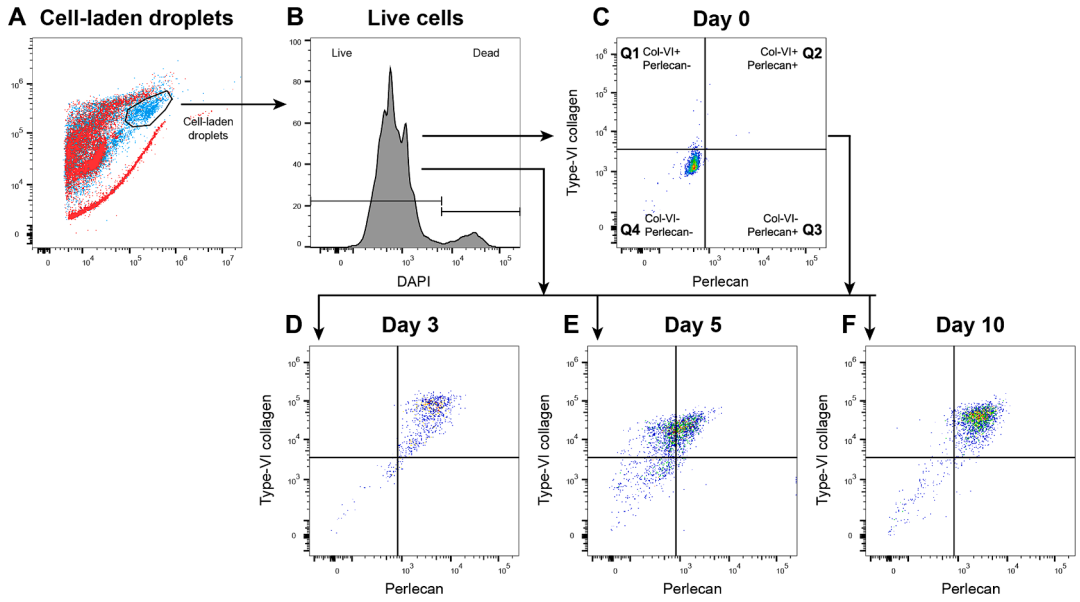

Fig. 9. Schematic overview of the gating strategy to analyze the flow cytometry data. A: Dot plot comparing droplets without (red) and with (blue) cells. The events of the cell-laden sample not overlapping with the events from the empty batch are considered cell-laden droplets. B: Histogram of DAPI staining of cell-laden microgels with gating to discriminate between live and dead cells. C: Type-VI collagen and perlecan staining of live cells at day 0. Quad gates are determined by assuming that there is no matrix present on day 0. The quad gates are copied to later time points of the same donor (D-F). (For interpretation of the references to color in this figure legend, the reader is referred to the web version of this article.)

structural parameters of the PCM, a semi-quantitative analysis was performed on the microscopy images using CellProfiler (v 4.2.6, Broad Institute, Cambridge, Massachusetts, United States). The PCM thickness with respect to the cell nucleus and the percentage of PCM coverage per nucleus were determined (Fig. 6A).

Statistical analysis

All datasets were tested for normal distributions using a Shapiro-Wilk normality test ($p < 0.05$). Parametric tests were used when the dataset was normally distributed, otherwise nonparametric tests were used. To compare droplet diameters of ACs and ACPCs, an independent *t*-test was used. The mean differences in cell viability between culture duration and cell type were compared using a two-way ANOVA with a Tukey multiple comparisons post-hoc test. Timepoints were compared with a repeated measures one-way ANOVA, or a mixed-effects analysis for datasets with missing datapoints, and a Tukey multiple comparisons post-hoc test. Datasets that did not pass the Shapiro-Wilk test were compared with a Friedman test for repeated measures or a Kruskal-Wallis test and Dunn's multiple comparisons post-hoc test. ACs and ACPCs were compared using an independent *t*-test or a Mann-Whitney test. Data are presented as mean (±standard deviation) and significance was set at $p < 0.05$. All statistical analyses were performed with GraphPad Prism (v 8.0.2, San Diego, CA).

Funding sources

This work was financially supported by the Gravitation Program "Materials Driven Regeneration", funded by the Netherlands Organization for Scientific Research (024.003.013) and the European Research Council (ERC) under the European Union's Horizon 2020 research and innovation program (grant agreement No. 802791).

CRediT authorship contribution statement

Marloes van Mourik: Writing – review & editing, Writing – original draft, Visualization, Validation, Project administration, Methodology, Investigation, Formal analysis, Conceptualization. **Bart M. Tiemeijer:** Writing – review & editing, Resources, Methodology, Investigation. **Maarten van Zon:** Writing – review & editing, Validation, Methodology, Investigation. **Florencia Abinzano:** Writing – review & editing, Resources, Methodology. **Jurjen Tel:** Supervision, Resources, Funding acquisition. **Jasper Foolen:** Writing – review & editing, Supervision, Funding acquisition, Conceptualization. **Keita Ito:** Writing – review & editing, Supervision, Funding acquisition, Conceptualization.

Declaration of competing interest

The authors declare that they have no known competing financial interests or personal relationships that could have appeared to influence the work reported in this paper.

Data availability

Data will be made available on request.

Acknowledgments

The authors thank Jet Peters and Amer Banda for providing support during sample production.

Appendix A. Supplementary data

Supplementary data to this article can be found online at https://doi.org/10.1016/j.mbplus.2024.100157.

References

[1] R. Stahl, S.K. Jain, J. Lutz, B.T. Wyman, M.-P. Hellio Le Graverand-Gastineau, E. Vignon, S. Majumdar, T.M. Link, Osteoarthritis of the knee at 3.0 T: comparison of a quantitative and semi-quantitative score for the assessment of the extent of cartilage lesion and bone marrow edema pattern in a 24-month longitudinal study, Skeletal Radiol. 40 (2011) 1315–1327.

[2] G.W. Knutsen, J.O. Drogset, L. Engebretsen, T. Grøntvedt, V. Isaksen, T. C. Ludvigsen, S. Roberts, E. Solheim, T. Strand, O. Johansen, G.W. Knutsen, J. O. Drogset, L. Engebretsen, T. Grøntvedt, V. Isaksen, T.C. Ludvigsen, A randomized trial comparing autologous chondrocyte implantation with microfracture: Findings at five years, J. Bone Joint Surg. Am. 89 (2007) 2105–2112.

[3] J.D. Harris, R.A. Siston, R.H. Brophy, C. Lattermann, J.L. Carey, D.C. Flanigan, Failures, re-operations, and complications after autologous chondrocyte implantation - a systematic review, Osteoarthr. Cartil. 19 (2011) 779–791.
[4] A.R. Armiento, M. Alini, M.J. Stoddart, Articular fibrocartilage - Why does hyaline cartilage fail to repair? Adv. Drug Deliv. Rev. 146 (2019) 289–305.
[5] J. Parreno, M. Nabavi Niaki, K. Andrejevic, A. Jiang, P.-H.-H. Wu, R.A. Kandel, Interplay between cytoskeletal polymerization and the chondrogenic phenotype in chondrocytes passaged in monolayer culture, J. Anat. 230 (2017) 234–248.
[6] L.A. Vonk, B.Z. Doulabi, C. Huang, M.N. Helder, V. Everts, R.A. Bank, Preservation of the chondrocyte's pericellular matrix improves cell-induced cartilage formation, J. Cell. Biochem. 110 (2010) 260–271.
[7] F. Guilak, L.G. Alexopoulos, M.L. Upton, I. Youn, J.B. Choi, L. Cao, L.A. Setton, M. A. Haider, The pericellular matrix as a transducer of biomechanical and biochemical signals in articular cartilage, Ann. N. Y. Acad. Sci. 1068 (2006) 498–512.
[8] J.B. Choi, I. Youn, L. Cao, H.A. Leddy, C.L. Gilchrist, L.A. Setton, F. Guilak, Zonal changes in the three-dimensional morphology of the chondron under compression: the relationship among cellular, pericellular, and extracellular deformation in articular cartilage, J. Biomech. 40 (2007) 2596–2603.
[9] M. Danalache, R. Kleinert, J. Schneider, A.L. Erler, M. Schwitalle, R. Riester, F. Traub, U.K. Hofmann, Changes in stiffness and biochemical composition of the pericellular matrix as a function of spatial chondrocyte organisation in osteoarthritic cartilage, Osteoarthr. Cartil. 27 (2019) 823–832.
[10] L.G. Alexopoulos, L.A. Setton, F. Guilak, The biomechanical role of the chondrocyte pericellular matrix in articular cartilage, Acta Biomater. 1 (2005) 317–325.
[11] R.E. Wilusz, L.E. Defrate, F. Guilak, A biomechanical role for perlecan in the pericellular matrix of articular cartilage, Matrix Biol, J. Int. Soc. Matrix Biol. 31 (2012) 320–327.
[12] F. Guilak, R.J. Nims, A. Dicks, C.-L. Wu, I. Meulenbelt, Osteoarthritis as a disease of the cartilage pericellular matrix, Matrix Biol. 71–72 (2018) 40–50.
[13] Z. Zhang, Chondrons and the pericellular matrix of chondrocytes, Tissue Eng. - Part B Rev. 21 (2015) 267–277.
[14] L.A. Vonk, T.S. de Windt, A.H.M. Kragten, M. Beekhuizen, S.C. Mastbergen, W.J. A. Dhert, F.P.J.G. Lafeber, L.B. Creemers, D.B.F. Saris, Enhanced cell-induced articular cartilage regeneration by chondrons; the influence of joint damage and harvest site, Osteoarthr. Cartil. 22 (2014) 1910–1917.
[15] T.F.F. Saris, T.S. de Windt, E.C. Kester, L.A. Vonk, R.J.H. Custers, D.B.F. Saris, Five-year outcome of 1-stage cell-based cartilage repair using recycled autologous chondrons and allogenic mesenchymal stromal cells: A first-in-human clinical trial, Am. J. Sports Med. 49 (2021) 941–947.
[16] W. Duan, Y. Zhao, X. Ren, R. Zhao, Q. Li, Z. Sun, W. Song, Y. Yang, P. Li, X. Wei, Combination of chondrocytes and chondrons improves extracellular matrix production to promote the repairs of defective knee cartilage in rabbits, J. Orthop. Transl. 28 (2021) 47–54.
[17] M. van Mourik, G.H. Schuiringa, L.P. Varion-Verhagen, L.A. Vonk, C.C. Van Donkelaar, K. Ito, J. Foolen, Enzymatic isolation of articular chondrons: is it much different than that of chondrocytes? Tissue Eng. - Part C Methods 29 (2023) 30–40.
[18] H.C. Peters, T.J. Otto, J.T. Enders, W. Jin, B.R. Moed, Z. Zhang, The protective role of the pericellular matrix in chondrocyte apoptosis, Tissue Eng. - Part A 17 (2011) 2017–2024.
[19] G.M. Lee, C.A. Poole, S.S. Kelley, J. Chang, B. Caterson, Isolated chondrons: a viable alternative for studies of chondrocyte metabolism in vitro, Osteoarthr. Cartil. 5 (1997) 261–274.
[20] E.D. Aldrich, X. Cui, C.A. Murphy, K.S. Lim, G.J. Hooper, C.W. McIlwraith, T.B. F. Woodfield, Allogeneic mesenchymal stromal cells for cartilage regeneration: A review of in vitro evaluation, clinical experience, and translational opportunities, Stem Cells Transl. Med. 10 (2021) 1500–1515.
[21] M.K. Mamidi, A.K. Das, Z. Zakaria, R. Bhonde, Mesenchymal stromal cells for cartilage repair in osteoarthritis, Osteoarthr. Cartil. 24 (2016) 1307–1316.
[22] L. Bian, D.Y. Zhai, R.L. Mauck, J.A. Burdick, Coculture of human mesenchymal stem cells and articular chondrocytes reduces hypertrophy and enhances functional properties of engineered cartilage, Tissue Eng. - Part A 17 (2011) 1137–1145.
[23] I.M. Khan, J.C. Bishop, S. Gilbert, C.W. Archer, Clonal chondroprogenitors maintain telomerase activity and Sox9 expression during extended monolayer culture and retain chondrogenic potential, Osteoarthr. Cartil. 17 (2009) 518–528.
[24] G.P. Dowthwaite, J.C. Bishop, S.N. Redman, I.M. Khan, P. Rooney, D.J.R.R. Evans, L. Haughton, Z. Bayram, S. Boyer, B. Thomson, M.S. Wolfe, C.W. Archer, The surface of articular cartilage contains a progenitor cell populations, J. Cell Sci. 117 (2004) 889–897.
[25] Y. Jiang, Y. Cai, W. Zhang, Z. Yin, C. Hu, T. Tong, P. Lu, S. Zhang, D. Neculai, R. S. Tuan, H.W. Ouyang, Human cartilage-derived progenitor cells from committed chondrocytes for efficient cartilage repair and regeneration, Stem Cells Transl. Med. 5 (2016) 733–744.
[26] R. Levato, W.R. Webb, I.A. Otto, A. Mensinga, Y. Zhang, M. van Rijen, R. van Weeren, I.M. Khan, J. Malda, The bio in the ink: cartilage regeneration with bioprintable hydrogels and articular cartilage-derived progenitor cells, Acta Biomater. 61 (2017) 41–53.
[27] D.E. Anderson, B.D. Markway, K.J. Weekes, H.E. McCarthy, B. Johnstone, Physioxia promotes the articular chondrocyte-like phenotype in human chondroprogenitor-derived self-organized tissue, Tissue Eng. - Part A 24 (2018) 264–274.
[28] H.A. Owida, N.L. Kuiper, Y. Yang, Maintenance and acceleration of pericellular matrix formation within 3D cartilage cell culture models, Cartilage 13 (2021) 847S–S861.
[29] B.M. Tiemeijer, L. Descamps, J. Hulleman, J.J.F. Sleeboom, J. Tel, A microfluidic approach for probing heterogeneity in cytotoxic T-cells by cell pairing in hydrogel droplets, Micromachines 13 (2022) 1–14.
[30] B.J. Morgan, G. Bauza-Mayol, O.F.W. Gardner, Y. Zhang, R. Levato, C.W. Archer, R. Van Weeren, J. Malda, R.S. Conlan, L.W. Francis, I.M. Khan, Bone morphogenetic protein-9 is a potent chondrogenic and morphogenic factor for articular cartilage chondroprogenitors, Stem Cells Dev. 29 (2020) 882–894.
[31] K. Padmaja, S. Manickam, A. Grace, S. Sathishkumar, E. Vinod, Supplementation of articular cartilage - derived chondroprogenitors with bone morphogenic protein - 9 enhances chondrogenesis without affecting hypertrophy, Biotechnol. Lett. (2022).
[32] J. Chang, C.A. Poole, Confocal analysis of the molecular heterogeneity in the pericellular microenvironment produced by adult canine chondrocytes cultured in agarose gel, Histochem. J. 29 (1997) 515–528.
[33] S.A. Fraser, A. Crawford, A. Frazer, S. Dickinson, A.P. Hollander, I.M. Brook, P. V. Hatton, Localization of type VI collagen in tissue-engineered cartilage on polymer scaffolds, Tissue Eng. 12 (2006) 569–577.
[34] F. Verrecchia, M. Chu, A. Mauviel, Identification of novel TGF-beta/smad gene targets in dermal fibroblasts using a combined cDNA microarray/promoter transactivation approach, J. Biol. Chem. 276 (2001) 17058–17062.
[35] R.E. Wilusz, J. Sanchez-Adams, F. Guilak, The structure and function of the pericellular matrix of articular cartilage, Matrix Biol. 39 (2014) 25–32.
[36] J.P. Fredrikson, P.P. Brahmachary, A.E. Erdoğan, Z.K. Archambault, J.N. Wilking, R.K. June, C.B. Chang, Metabolomic profiling and mechanotransduction of single chondrocytes encapsulated in alginate microgels, Cells 11 (2022).
[37] J.P. Fredrikson, P.P. Brahmachary, R.K. June, L.M. Cox, C.B. Chang, Pericellular matrix formation and atomic force microscopy of single primary human chondrocytes cultured in alginate microgels, Adv. Biol. 2300268 (2023) 1–10.
[38] P.M. van der Kraan, E.N. Blaney Davidson, A. Blom, W.B. van den Berg, TGF-beta signaling in chondrocyte terminal differentiation and osteoarthritis. Modulation and integration of signaling pathways through receptor-Smads, Osteoarthr. Cartil. 17 (2009) 1539–1545.
[39] V. Dexheimer, J. Gabler, K. Bomans, T. Sims, G. Omlor, W. Richter, Differential expression of TGF-β superfamily members and role of Smad1/5/9-signalling in chondral versus endochondral chondrocyte differentiation, Sci. Rep. 6 (2016) 1–14.
[40] M.M. Maples, M.C. Schneider, S.J. Bryant, Impact of inter- and intra-donor variability by age on the gel-to-tissue transition in MMP-sensitive PEG hydrogels for cartilage regeneration, ACS Appl. Bio Mater. 6 (2023) 2677–2689.
[41] E. Delve, V. Co, R.A. Kandel, Superficial and deep zone articular chondrocytes exhibit differences in actin polymerization status and actin-associated molecules in vitro, Osteoarthr. Cartil. Open 2 (2020) 100071.
[42] E. Vinod, R. Parameswaran, S.M. Amirtham, G. Rebekah, U. Kachroo, Comparative analysis of human bone marrow mesenchymal stem cells, articular cartilage derived chondroprogenitors and chondrocytes to determine cell superiority for cartilage regeneration, Acta Histochem. 123 (2021).
[43] M. Rikkers, J.V. Korpershoek, R. Levato, J. Malda, L.A. Vonk, The clinical potential of articular cartilage-derived progenitor cells: a systematic review, NPJ Regen. Med. 7 (2022) 2.
[44] N. Sinha, N. Subedi, F. Wimmers, M. Soennichsen, J. Tel, A pipette-tip based method for seeding cells to droplet microfluidic platforms, J. Vis. Exp. 1–10 (2019).
[45] D.J. Collins, A. Neild, A. deMello, A.Q. Liu, Y. Ai, The Poisson distribution and beyond: Methods for microfluidic droplet production and single cell encapsulation, Lab Chip 15 (2015) 3439–3459.
[46] S. ten Klooster, S. Sahin, K. Schroën, Monodisperse droplet formation by spontaneous and interaction based mechanisms in partitioned EDGE microfluidic device, Sci. Rep. 9 (2019) 1–12.